The Astrophysical Journal, 520:L139–L142, 1999 August 1

SOHO EIT OBSERVATIONS OF EXTREME-ULTRAVIOLET "DIMMING" ASSOCIATED WITH A HALO CORONAL MASS EJECTION

Dominic M. Zarro,[1] Alphonse C. Sterling,[2,3] Barbara J. Thompson,[4] Hugh S. Hudson,[3,5] and Nariaki Nitta[6]

Received 1999 February 5; accepted 1999 May 12; published 1999 June 25

ABSTRACT

A solar flare was observed on 1997 April 7 with the Soft X-ray Telescope (SXT) on *Yohkoh*. The flare was associated with a "halo" coronal mass ejection (CME). The flaring region showed areas of reduced soft X-ray (SXR) brightness—"dimmings"—that developed prior to the CME observed in white light and persisted for several hours following the CME. The most prominent dimming regions were located near the ends of a preflare SXR S-shaped (sigmoid) feature that disappeared during the event, leaving behind a postflare SXR arcade and cusp structure. Based upon these and similar soft X-ray observations, it has been postulated that SXR dimming regions are the coronal signatures (i.e., remnants) of magnetic flux ropes ejected during CMEs. This Letter reports new observations of coronal dimming at extreme-ultraviolet (EUV) wavelengths obtained with the Extreme-ultraviolet Imaging Telescope (EIT) on the *Solar and Heliospheric Observatory* (*SOHO*). A series of EIT observations in the 195 Å Fe xii wavelength band were obtained simultaneously with SXT during the 1997 April 7 flare/CME. The EIT observations show that regions of reduced EUV intensity developed at the same locations and at the same time as SXR dimming features. The decrease in EUV intensity (averaged over each dimming region) occurred simultaneously with an increase in EUV emission from flaring loops in the active region. We interpret these joint observations within the framework of flux-rope eruption as the cause of EUV and SXR coronal dimmings, and as the source of at least part of the CME.

Subject headings: Sun: corona — Sun: flares — Sun: UV radiation — Sun: X-rays, gamma rays

1. INTRODUCTION

Regions of reduced soft X-ray (SXR) emission associated with coronal mass ejections (CMEs) have been observed with the Soft X-ray Telescope (SXT) on *Yohkoh* (Sterling & Hudson 1997; Gopalswamy & Hanaoka 1998) and have been reported in *Skylab* X-ray data (Rush & Hildner 1976). These regions, termed coronal "dimmings," develop on a typical timescale of an hour and can persist for several days. The evolution timescale of coronal dimmings is faster than typical radiative cooling timescales in the corona, indicating that density depletion via expansion or ejection is most likely responsible for the dimming process (Hudson, Acton, & Freeland 1996).

In some cases, dimming regions are associated spatially with preflare active region magnetic structures that have a sheared sigmoid shape (Hudson et al. 1998; Canfield, Hudson, & McKenzie 1999). During the CME, the sigmoid structure evolves into a bright SXR cusp-shaped loop arcade structure—a structure often presented as observational evidence for reconnected magnetic fields following the eruption. Based on these observed characteristics, it is speculated that SXR coronal dimmings are the remnant signatures of the eruption of large-scale magnetic flux ropes that occurs during CMEs (Hudson & Webb 1997).

This Letter further investigates coronal dimming and associated arcade restructuring by comparing SXT observations of the 1997 April 7 flare/CME with simultaneous observations at 195 Å obtained with the Extreme-ultraviolet Imaging Telescope (EIT) on the *Solar and Heliospheric Observatory* (*SOHO*). Radiation at this extreme-ultraviolet (EUV) wavelength is dominated by Fe xii emission lines that are characteristically formed at about 1.5×10^6 K. Consequently, EUV imaging at these relatively cool temperatures probes different coronal regions than observed with higher temperature ($\gtrsim 3 \times 10^6$ K) SXR imaging.

2. OBSERVATIONS

The 1997 April 7 flare was a *GOES*-class C6.8 long-duration event (LDE) that commenced at approximately 13:50 UT in NOAA active region 8027. The flare was associated with a "halo" CME observed by the *SOHO* Large Angle Spectroscopic Coronagraph (LASCO) at 14:27 UT (Michels et al. 1997) and was associated also with a large-scale wavelike disturbance that was detected in EIT full-disk images (Thompson et al. 1999). This event was studied by Sterling & Hudson (1997), who found evidence for coronal dimming and arcade-cusp formation in SXT observations.

2.1. *Sigmoid*

EIT 195 Å full-disk observations were obtained during the flare at intervals of approximately 9–18 minutes. Figures 1*a* and 1*b* compare preflare SXT AlMg and EIT images of the active region at 13:28:42 UT and 13:28:23 UT, respectively. As noted by Sterling & Hudson (1997), the preflare active region in SXRs is characterized by a bright sigmoid-shaped structure that is morphologically similar to the helically kinked magnetic flux features that are often associated with CMEs (Rust & Kumar 1996). The preflare EUV image shows an overall active region morphology that is similar to that observed by SXT. However, at EUV wavelengths, the sigmoid location

[1] SM&A Systems Solutions Group at NASA Goddard Space Flight Center, Code 682.3, Greenbelt, MD 20771; dzarro@solar.stanford.edu.

[2] Computational Physics, Inc., 2750 Prosperity Avenue, Fairfax, VA 22031; sterling@isasxa.solar.isas.ac.jp. Also, E. O. Hulburt Center for Space Research, Naval Research Laboratory, Washington, DC.

[3] Current address: Institute for Space and Astronautical Science, Yoshinodai 3-1-1, Sagamihara, Kanagawa 229, Japan.

[4] NASA Goddard Space Flight Center, Code 682, Greenbelt, MD 20771; barbara.thompson@gsfc.nasa.gov.

[5] Solar Physics Research Corp., 4720 Calle Desecada, Tucson, AZ 85718; hudson@isass1.solar.isas.ac.jp.

[6] Lockheed Martin Solar and Astrophysics Laboratory, 3251 Hanover Street, Palo Alto, CA 94304; nitta@1msal.com.

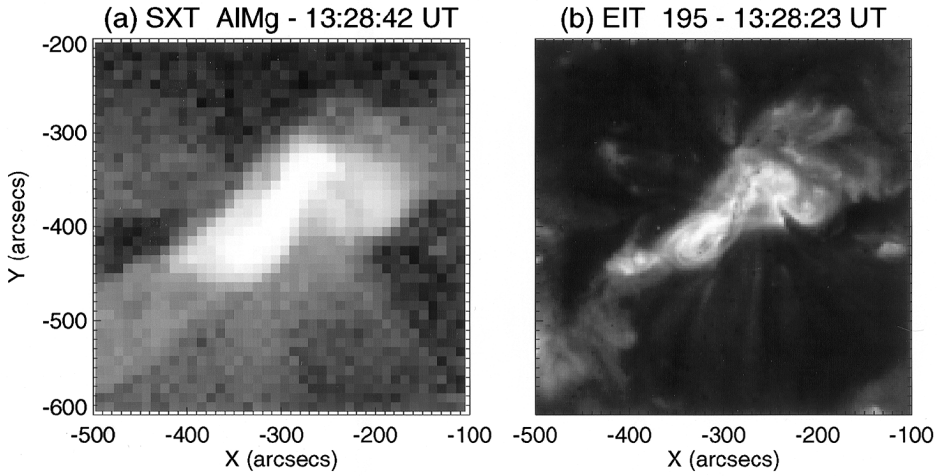

Fig. 1.—(*a*) SXT AlMg filter image obtained at 13:28:42 UT, approximately 30 minutes before flare maximum. Pixel resolution is 9.″82. SXR emission appears as a bright sigmoid-shaped structure. The image has been dark-current subtracted, exposure normalized, corrected for spacecraft jitter, and corrected for a ~1° roll. (*b*) EIT 195 Å filter image obtained at 13:28:23 UT, approximately 20 s before the SXT preflare image in Fig. 1*a*. Pixel resolution is 2.″56.

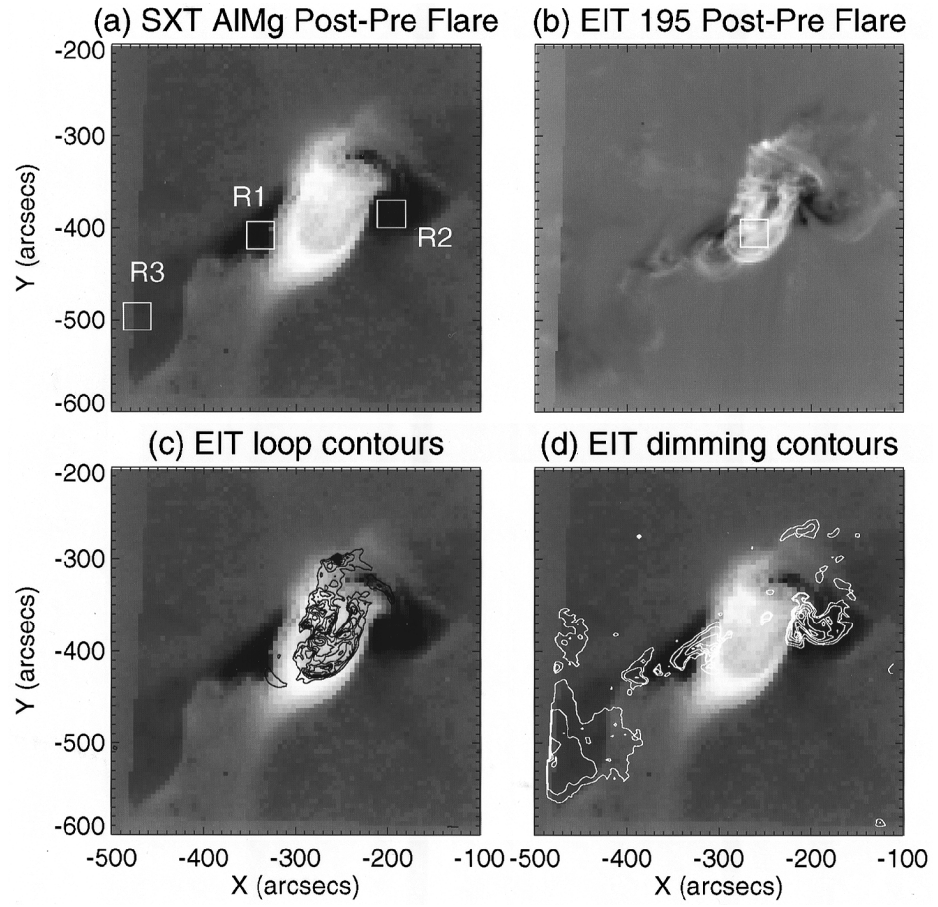

Fig. 2.—(*a*) Difference image derived by subtracting SXT preflare image from postflare image, after correction for solar rotation. Two SXR dimming regions (R1 and R2) lie diagonally to either side of a bright arcade-cusp structure. A third less prominent dimming region (R3) appears southeast of R1. The square boxes denote 30″ × 30″ areas used for computing intensity light curves in Fig. 4. (*b*) Difference image derived by subtracting EIT preflare image from postflare image, after correction for solar rotation. Two EUV dimming regions located diagonally to either side of the EUV loops correspond closely to SXR dimming regions R1 and R2. A third EUV dimming region is evident in the vicinity of SXR dimming region R3. (*c*) Overlay of positive intensity contours from EIT difference image on SXT difference image. EUV loops lie within envelope defined by the SXR arcade-cusp emission. (*d*) Overlay of negative intensity contours from EIT difference image on SXT difference image. EUV dimming regions map closely the SXR dimming regions.

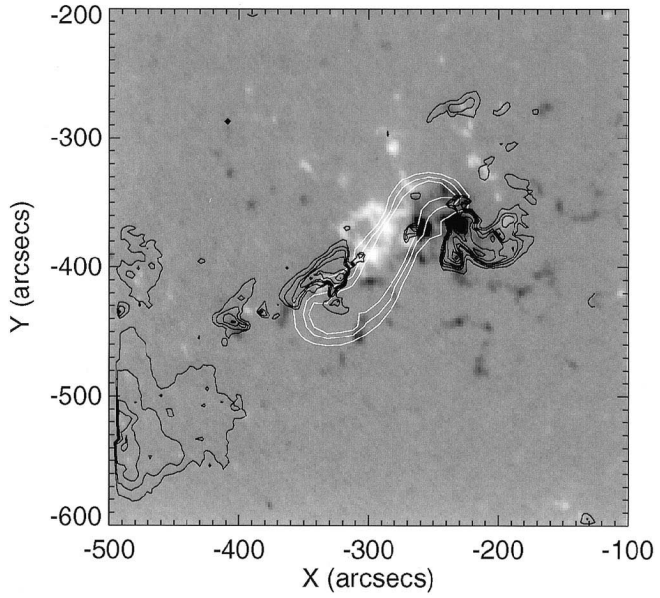

Fig. 3.—Overlay of SXT preflare sigmoid structure (*white contour*) and EIT dimming regions (*black contour*) on MDI magnetogram at 1997 April 7 14:27:03 UT.

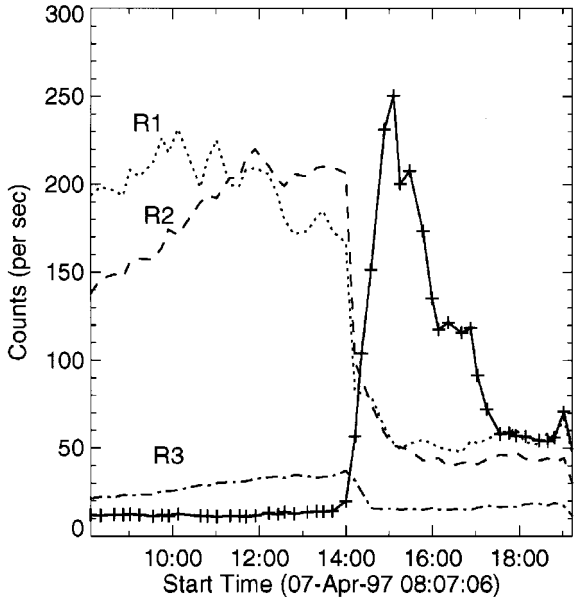

Fig. 4.—EIT 195 Å dimming light curves (*dashed, dotted, and dot-dashed lines*) computed from the average intensity in 30″ × 30″ areas centered on regions R1, R2, and R3. EUV flare light curve (*solid line*) computed from the average intensity in a 30″ × 30″ area centered on the EUV postflare loop apex (Fig. 2*b*). Temporal resolution varies between 9 and 18 minutes. Flare count rates have been reduced by a factor of 5 for comparison with dimming region count rates. Because of saturation effects in the EIT detector at the peak of the flare, the 195 Å count rate at flare maximum is reduced from its actual value.

is composed predominantly of smaller scale loop structures that emanate from the active region and which are not visible in SXRs. A dark EUV structure is aligned along the center portion of the SXT sigmoid. This feature appears to be spatially associated with a preflare filament observed in Big Bear Solar Observatory (BBSO) Hα images.

Postflare SXT and EIT images show dramatic changes in the active region morphology, suggesting a restructuring of magnetic fields. We illustrate these changes via difference images. Figures 2*a* and 2*b* show SXT and EIT difference images computed by subtracting the preflare images in Figure 1 from corresponding postflare images at 17:40:40 UT and 17:46:19 UT, respectively. The differences were computed by rotating the preflare image to the time of the postflare image and rebinning to a common spatial scale to ensure the proper subtraction of matching pixels. We used the solar differential rotation formula of Howard, Harvey, & Forgach (1990) to rotate the preflare images. As found originally by Sterling & Hudson (1997), the SXT difference image (Fig. 2*a*) shows that the preflare sigmoid feature has disappeared and is replaced by a bright postflare cusp-shaped arcade structure at approximately the same location. The disappearance of the sigmoid is temporally associated with a filament eruption from the active region that was recorded during the interval 13:44–13:55 UT in NOAA Solar-Geophysical Data. Examination of postflare BBSO images at 16:00 UT indicates that part of the filament was still present at the sigmoid location, suggesting that not all of the filament erupted (or that it had reformed a short time later). The EIT difference image (Fig. 2*b*) shows a set of bright approximately semicircular EUV loops that connect across the location of the preflare SXR sigmoid. The central portion of the EUV loops shows dark EUV material which likely corresponds to the unerupted portion of the Hα filament.

Bright cusp structures have been observed by SXT in LDE flares and also in the quiet Sun and nonflaring active regions (Yoshida & Tsuneta 1996). Within the limits of confusion caused by geometrical projection effects, a cusp structure indicates oppositely directed field lines in the corona and, hence, implies possible reconnection occurring at or above the loop apex (see, e.g., Tsuneta 1996). Coalignment of the EIT and SXT difference images indicates that (cooler) EUV postflare loops are physically distinct from the (hotter) SXR arcade-cusp and that a cusp structure is not evident in EUV postflare emission. This distinction is illustrated in Figure 2*c* in which positive values in the EIT difference image are overlaid as contours onto the SXT difference image. The EUV contours appear as rounded features confined predominantly within an envelope of SXR emission outlined by the arcade-cusp.

2.2. *Dimming*

Figure 2*a* shows two SXR dimming regions (marked R1 and R2) that extend diagonally away from the footpoints of the SXR cusp. A third weaker dimming region (R3) is also apparent southeast of the cusp. Figure 2*b* shows two similar EUV dimming regions located near the footpoints of the EUV postflare loops. The locations of the EUV dimming regions match closely those of the SXR dimming regions. This correspondence is demonstrated in Figure 2*d*, in which negative contour levels for the EIT difference image are overlaid on the SXT difference image. The third weaker SXR dimming region (R3) also appears spatially associated with a weak EUV dimming region.

Photospheric magnetograms from the *SOHO* Michelson Doppler Imager (MDI) were obtained at approximately 1.5 hr intervals during the flare/CME. The MDI images show a magnetically complex active region that was not simply bipolar but consisted of intermingled mixed polarities. Figure 3 shows a contour overlay of the preflare SXT image from Figure 1*a* on an MDI image obtained shortly after SXR flare maximum at 14:27:03 UT. For comparison, contours of the EUV dimming

regions from Figure 2*b* are also overlaid on the magnetogram. The overlay confirms the findings of Sterling & Hudson (1997), namely, that the main body of the preflare sigmoid is aligned approximately along the magnetic neutral line. The EUV overlay shows that the apparent ends of the SXR sigmoid terminate at the boundaries of the two EUV dimming regions R1 and R2. It is difficult to assess the dominant polarity in either of these dimming regions; however, it appears that the EUV (and by implication SXR) dimming regions have opposite polarities near the edges closest to the active region (and preflare sigmoid). Away from these edges, the dimming regions are not associated with regions of strong photospheric magnetic field or prevailing magnetic polarity.

Figure 4 shows the average count rate in a $30'' \times 30''$ area centered on the postflare EIT loop apex in Figure 2*b*. The light curve shows a rapid rise and decay, typical of transition region EUV emission in flares (cf. Woodgate et al. 1983). The flare light curve is compared with the average count rates in similar-sized areas centered on regions R1, R2, and R3 (indicated by the boxes in Fig. 2*a*). Each region shows approximately a factor of 2–4 decrease in average intensity that occurs simultaneously (to within instrument temporal resolution limits) with the increase in loop apex intensity during the flare. A similar temporal coincidence between CME dimming onset and arcade loop brightening was also reported in SXT observations of a dimming event studied by Hudson & Webb (1997).

3. CONCLUSION

Hudson & Webb (1997) identified four classes of coronal SXR dimming signatures: *dimming above an LDE flare*, *cloud ejections*, *envelope dimmings*, and *transient coronal holes*. The observations of the 1997 April 7 event are consistent with the transient coronal hole category, in which regions near a coronal arcade undergo a relatively rapid decrease to brightness values that approach coronal hole levels. This flare had also the properties of an LDE with an associated halo CME. The SXR dimming appeared on diagonally opposite sides of a sigmoid-shaped loop structure that developed before the flare and evolved into an arcade-cusp structure after the flare (and CME). This sequence of events led Sterling & Hudson (1997) to conclude that the SXR dimming regions were the remnants of a double-lobed loop ejection that occurred during the CME. The observation of simultaneous and cospatial dimming at the cooler ($<2 \times 10^6$ K) temperatures characteristic of EUV emission supports the latter interpretation. The EUV dimming observations suggest that magnetic destabilizations associated with a CME extend into cooler coronal layers than indicated by SXR observations and that coronal dimmings are more likely caused by density depletion (and/or volume expansion) rather than a temperature variation in the coronal plasma. Such density depletion is a key feature of flux-rope eruption models of CMEs in which coronal material is evacuated during the expansion and opening of magnetic field lines. The observed spatial correspondence between EUV dimming locations and regions of opposite magnetic polarity near the edges of the preflare sigmoid is consistent with these dimming regions marking the evacuated feet of the magnetic lobes of the sigmoid.

The present observations raise important issues to be addressed by reconnection models of solar flares. For example, the observed close temporal coincidence between CME dimming onset and flare loop brightening is inconsistent with standard CME models that involve large-scale reconnection following ideal MHD instabilities. The latter models predict that the flare loop brightening would be delayed with respect to the CME onset (cf. Kopp & Pneuman 1976; Forbes & Priest 1982). A related issue is why a cusp structure is not prominent in postflare EUV emission. Recent CME modeling results by Antiochos (1998) and Antiochos, DeVore, & Klimchuk (1999) are of particular relevance to addressing such issues. According to these simulations, the additional flux systems associated with regions of mixed magnetic polarity (such as in the present flaring active region) are necessary to enable reconnection between overlying unsheared flux and neighboring field lines. This reconnection triggers eruption or "break out" of the underlying sheared field (i.e., SXR sigmoid), leaving behind closed lower lying loops such as the observed noncusp EUV postflare loops. Future investigations of simultaneous EUV/SXR dimming and postflare loop brightening in flare/CMEs will provide new tests of predictions made by different flare reconnection and eruption models.

The work described in this Letter was commenced at the Third *Yohkoh/SOHO* Coordinated Data Analysis Workshop (CDAW) held at ISAS, Japan, during 1998 April 6–10. D. M. Z. was supported by NAS5-32350. A. C. S. received support from the NRL/ONR basic research program. H. S. H. and N. N. were supported by NASA grant NAS8-40801.

REFERENCES

Antiochos, S. K. 1998, ApJ, 502, L181
Antiochos, S. K., DeVore, C. R., & Klimchuk, J. A. 1999, ApJ, 510, 485
Canfield, R. C., Hudson, H. S., & McKenzie, D. E. 1999, Geophys. Res. Lett., 26(6), 627
Forbes, T. G., & Priest, E. R. 1982, Sol. Phys., 135, 361
Gopalswamy, N., & Hanaoka, Y. 1998, ApJ, 498, L179
Howard, R. A., J. Harvey, & Forgach, P. 1990, Sol. Phys., 130, 295
Hudson, H. S., Acton, L. W., & Freeland, S. L. 1996, ApJ, 470, 629
Hudson, H. S., Lemen, J. R., St. Cyr, O. C., Sterling, A. C., & Webb, D. F. 1998, Geophys. Res. Lett., 25(14), 248
Hudson, H. S., & Webb, D. F. 1997, Geophysical Monographs 99, Coronal Mass Ejections, ed. N. Crooker, J. Joselyn, & J. Feynman (Washington, DC: AGU), 27
Kopp, R. A., & Pneuman, G. W. 1976, Sol. Phys., 50, 85
Michels, D. J., et al. 1997, Eos Trans. AGU, 78, S274
Rust, D. M., & Hildner, E. 1976, Sol. Phys., 48, 381
Rust, D. M., & Kumar, A. 1996, ApJ, 464, L199
Sterling, A. C., & Hudson, H. S. 1997, ApJ, 491, L55
Thompson, B. J., et al. 1999, ApJ, 517, L151
Tsuneta, S. 1996, ApJ, 456, 840
Woodgate, B. E., Shine, R. A., Poland, A. I., & Orwig, L. E. 1983, ApJ, 265, 530
Yoshida, T., & Tsuneta, S. 1996, ApJ, 459, 342